Proceedings of the ASME 2025 44th International Conference on Ocean, Offshore and Arctic Engineering
OMAE2025
June 22-27 2025, Vancouver, British Columbia, Canada

OMAE2025-156361

GLOBAL AND LOCAL RESPONSE OF SUBMERGED FLOATING TUNNELS TO HYDRODYNAMIC LOADS

Stefano Corazza[1,*], Francesco Foti[1], Luca Martinelli[1] , Vincent Denoël[2]

[1]Department of Civil and Environmental Engineering, Politecnico di Milano, Italy
[2]Structural & Stochastic Dynamics, Structural Engineering Division, University of Liège, Belgium

ABSTRACT

Seabed-anchored Submerged Floating Tunnels (SFTs) are structures made of watertight tubular segments, assembled together and kept floating under the water table by a spread system of anchoring elements (mooring system) connected to the seabed. A distinctive feature of the dynamic behavior of SFTs is the presence of both global vibration modes, that involve significant displacements of the tunnel and quasi-static displacements of the anchoring elements, and local modes, that mainly involve transverse vibrations of the anchors. Dominant global and local modes of the structure are typically associated to well-separated values of the natural frequencies. However, computationally efficient Finite Element (FE) models able to simultaneously capture the main features of both global and local vibration modes with the same degree of accuracy, are inherently hard to set up. To overcome this difficulty, a dynamic substructuring technique is here adopted. A separate modeling of the two main substructures is employed, involving (1) a Reduced Order Model (ROM) of the anchoring elements, which accounts for both geometrical nonlinearities and a generic form of supports motion, and (2) a continuous model which describes the submerged tube as an Euler-Bernoulli beam resting a non-homogeneous Winkler's bed. Both the global and the local response to hydrodynamic loads are then studied, within this novel framework, by considering the case study of the proposal for the Messina's strait SFT, in Italy.

Keywords: Submerged Floating Tunnels, Hydrodynamic Loads, Global Dynamics, Local Dynamics, Volterra Model

1. INTRODUCTION

Submerged Floating Tunnels (SFTs), also named Archimedes bridges, are underwater modular structures which are deemed to be a valuable option for crossing deep and long waterways, such as sea straits, fjords, bays and alpine lakes. Even though a first realization is still missing, a lot of preliminary design proposals have been developed, starting from the last decade of the past century [1–4]. SFTs consist of a water immersed tubular structure which is floating at a depth of around 20-50 m, both to ensure an adequate navigation clearance and to avoid excessive water pressure. They are kept fixed in position thanks to a spread system of supporting elements.

The main design parameter of SFTs is the so-called Buoyancy to Weight Ratio (BWR), i.e. the ratio between the buoyancy force and the self-weight per unit of length of the tunnel. Among a lot of different preliminary design proposals which have been reported in the literature, seabed-anchored Submerged Floating Tunnels seem to have established themselves as the most promising solutions. They are characterized by values of BWR greater than unity; hence, they are kept fixed under the water surface by means of a spread system of tensioned anchoring devices connected to the seabed, i.e., the mooring system. In order to satisfy the common requirements of being slender, axially stiff and very flexible in the transverse direction, the anchoring devices are usually realized with structural cables or tubular steel profiles (tethers) closely spaced along the tunnel length. The mooring system typically provides most of the stiffness to the SFT, while nearly the totality of the mass of the structure is concentrated along the tube. As a consequence, dominant global and local modes of the structure are associated to well-separated values of the natural frequencies. Moreover, due to their inherent flexibility, seabed-anchored SFTs are prone to the effect of dynamic loads, such as earthquakes, waves, currents and traffic. While structural analysis methods under seismic (see, e.g. [5–8]) and traffic (see, e.g. [9, 10]) loads seem to have recently reached a maturity stage, hydroelastic and hydrodynamic behavior of SFTs still require further investigations. In fact, hydrodynamic loads are deemed to be the most critical for serviceability and fatigue life assessments of the whole SFT, because of their consistent and cyclic nature. Nevertheless, extreme hydrodynamic events may also be of concern for the safety of the structure. Hence, this work aims to do a further step in this direction, focusing on the hydrodynamic behavior

*Corresponding author: stefano.corazza@polimi.it

of seabed-anchored SFTs. Furthermore, as recently highlighted in [11], the classification of the motion regimes of the SFT to hydrodynamic loads has revealed that the global dynamic response can be regarded as quasi-static. On the contrary, both direct and indirect excitation of the tethers have been found to occur, possibly leading to simple or parametric resonance phenomena. As a result of the peculiar behavior of this structural typology, a one-way dynamic coupling between the tube and the anchoring elements is found, with the consequent possibility of considering separately the global and local dynamic behavior whenever dealing with direct loading of the anchoring elements. This work is articulated as follows: Sec. 2 sets the basis for modeling the hydrodynamic loads, Sec. 3 deals with the global hydrodynamic response of the SFT, while Sec. 4 considers the local dynamic response of the tethers subject to the same loading conditions. Sec. 5 presents an application example for both cases, while Sec. 6 draws the conclusions of the work.

2. MODELING OF THE HYDRODYNAMIC LOADS

Hydrodynamic loadings acting on a SFT are usually modeled starting from the spectral representation of the wave elevation for a certain return period. A general analytical form of the deepwater surface wave energy spectrum reads (see e.g. [12, 13]):

$$S_\eta(\omega) = C_0|\omega|^{-m}\,\exp(-B\,|\omega|^{-n}) \tag{1}$$

where the coefficients C_0, B, m and n allow to uniquely define the spectrum. In the most widespread case, m and n are respectively set equal to 5 and 4, while several empirical expressions for C_0 and B have been proposed in the literature, based on experimental measurements. The Power Spectral Density (PSD) of the wave elevation can be expressed, according to Bretschneider, making reference to the following parameters:

$$C_0 = 0.0081\,g^2 \qquad B = 3.11/H_s^2 \tag{2}$$

where g is the gravity acceleration and H_s is the so-called significant wave height, which is defined as the arithmetic average of the highest one-third of the waves in a wave record [12]. The PSD of the water kinematic quantities (i.e., velocity and acceleration of the water particles stemming from the wave) are then related to the PSD of the wave elevation thanks to suitable transfer functions. In this work, the linear Airy wave theory is used. Accordingly, the water surface elevation at a given time t in a certain coordinate x can be expressed as:

$$\eta(x,t) = A\cos(kx-\omega t) \tag{3}$$

where A is the wave amplitude, k is the wave number and ω represents the circular frequency of the wave, given by $\omega = 2\pi/T$, being T the wave period. Water particle horizontal and vertical velocities are respectively given by [12, 13]:

$$u_h(x,z,t) = \frac{2\pi A}{T}\frac{\cosh(kz)}{\sinh(kd)}\cos(kx-\omega t) \tag{4}$$

$$u_v(x,z,t) = \frac{2\pi A}{T}\frac{\sinh(kz)}{\sinh(kd)}\sin(kx-\omega t) \tag{5}$$

being d the depth of the seabed, measured from the water table and z a vertical coordinate starting from the seabed and directed upward. Simple differentiation of the previous equations with respect to the time variable allows to express both the horizontal and vertical water particle acceleration:

$$\dot{u}_h(x,z,t) = \frac{4\pi^2 A}{T^2}\frac{\cosh(kz)}{\sinh(kd)}\sin(kx-\omega t) \tag{6}$$

$$\dot{u}_v(x,z,t) = -\frac{4\pi^2 A}{T^2}\frac{\sinh(kz)}{\sinh(kd)}\cos(kx-\omega t) \tag{7}$$

Additionally, the following linear dispersion relation holds:

$$\omega^2 = gk\tanh(kd) \tag{8}$$

Straightforward manipulations allow to express the PSD of the water kinematic quantities, in case of deep-water, as follows:

$$S_{u_h}(\omega,z) = \omega^2\left[\frac{\cosh(\omega^2 z/g)}{\cosh(\omega^2 d/g)}\right]^2 S_\eta(\omega) \tag{9}$$

$$S_{u_v}(\omega,z) = \omega^2\left[\frac{\sinh(\omega^2 z/g)}{\cosh(\omega^2 d/g)}\right]^2 S_\eta(\omega) \tag{10}$$

$$S_{\dot{u}_h}(\omega,z) = \omega^4\left[\frac{\cosh(\omega^2 z/g)}{\cosh(\omega^2 d/g)}\right]^2 S_\eta(\omega) \tag{11}$$

$$S_{\dot{u}_v}(\omega,z) = \omega^4\left[\frac{\sinh(\omega^2 z/g)}{\cosh(\omega^2 d/g)}\right]^2 S_\eta(\omega) \tag{12}$$

The PSD of the hydrodynamic load can be then expressed, in quite general terms, as:

$$S_F(\omega,z) = [RAO(\omega,z)]^2 S_\eta(\omega) \tag{13}$$

where the symbol RAO denotes the Response Amplitude Operator, which takes different forms depending on the chosen modeling assumptions for the load (see Sec. 3).

3. GLOBAL DYNAMICS

Let us make reference to Fig. 1 and consider a straight SFT of length L_T, with constant (transverse) bending stiffness EI_T, external diameter D_T and linear virtual mass γ_T. The latter accounts for the added mass effect of the water which is displaced by the tunnel during its motion, i.e. $\gamma_T = \gamma + C_A\rho_w\pi D_T^2/4$, being γ the structural linear mass, ρ_w the water density and C_A the added-mass coefficient, which depends on the tube cross-section. In the case of a circular cross-section, $C_A = 1$ is usually adopted (see e.g. [13]). The tube is anchored to the seabed through a mooring system, which counteracts the positive buoyancy and provides an elastic restraint to the transverse displacements of the tunnel. Whenever the spacing between adjacent anchoring points (Δ) is much smaller than the tunnel length (i.e. $\Delta/L_T \ll 1$), the stiffness per unit of length of the mooring system can be conveniently described by means of a smeared equivalent model (see [14]). It is worth noting that this amounts to model the SFT as an Euler-Bernoulli beam continuously supported by a non-uniform Winkler-type soil. Within this framework, neglecting both shear deformability effects and geometrical nonlinearities, planar transverse vibrations around the static equilibrium configuration of the

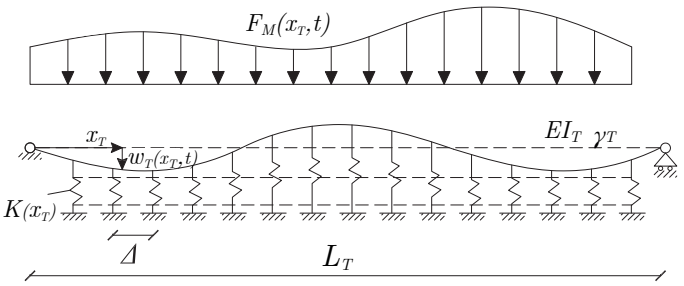

FIGURE 1: Structural model of the submerged tube as an Euler-Bernoulli beam on a Winkler's bed, subject to an in-plane dynamic force.

SFT are governed by the following partial differential equation (see [6, 14]):

$$EI_T \frac{\partial^4 w_T}{\partial x_T^4} + K(x_T) w_T + \gamma_T \frac{\partial^2 w_T}{\partial t^2} = F_M(x_T,t) - F_d(x_T,t) \quad (14)$$

where $x_T \in (0, L_T)$ and $t \in \mathbb{R}^+$ are, respectively, an abscissa spanning the length of the structure and the time variable, $w_T = w_T(x_T,t)$ is the transverse (flexural) displacement of the tunnel, $F_M(x_T,t)$ is a transverse distributed dynamic load, $F_d(x_T,t)$ is the damping force per unit of length of the tunnel and $K(x_T) = K_c \tilde{K}(x_T)$ describes the stiffness per unit of length of the mooring system, being $K_c > 0$ a characteristic stiffness value. Let us now investigate the hydrodynamic loading conditions, by expressing the dynamic load $F_M(x_T,t)$ according to the classical Morison formulation, superimposing the effect of both inertia and drag forces, as:

$$F_M(x_T,t) = F_I(x_T,t) + F_D(x_T,t) \quad (15)$$

where:

$$F_I(x_T,t) = C_I \rho_w \pi \frac{D_T^2}{4} \dot{u}_v(x_T, z^*, t) \quad (16)$$

and:

$$F_D(x_T,t) = \frac{1}{2} \rho_w C_D D_T |u_v(x_T, z^*, t)| u_v(x_T, z^*, t) \quad (17)$$

In the previous equation, the effect of a vertical current has been disregarded, as well as the structural velocity, considered negligible compared to the fluid velocity. The symbols C_I and C_D denote, respectively, the inertia and drag coefficient of the tube cross-section. It is also worth noting that, the loading on the SFT can be easily determined by computing the water kinematic quantities at a fixed depth, i.e. the tube's centroid depth ($z = z^*$), and assembling the corresponding PSD (cf. Eq. 13). Before proceeding, it is convenient to treat further the drag term, by applying a simple stochastic linearization, by exploiting the solution proposed by Borgman (see [15]):

$$|u_v(t)| u_v(t) = \sqrt{\frac{2}{\pi}} \sigma_{u_v} u_v(t) \quad (18)$$

where σ_{u_v} is the standard deviation of the vertical water velocity spectrum $S_{u_v}(\omega)$. Moreover, the water particle velocity is considered perfectly correlated along the tunnel's abscissa x_T, as a conservative choice, leading to a sole dependence of the Morison force upon the time variable, i.e. $F_M = F_M(t)$. From now on, let us also express the damping forces according to a classical hysteretic-type damping model:

$$F_d(x_T,t) = c_v \frac{\partial w_T}{\partial t} \quad (19)$$

where c_v is the viscous damping coefficient of the structure.

3.1 Non-dimensional formulation

The governing equations of the problem can be re-stated in non-dimensional form by introducing the non-dimensional space (ξ_T) and time (τ) variables:

$$\xi_T = \frac{x_T}{L_T} \qquad \tau = \Omega_c\, t \quad (20)$$

where the characteristic frequency Ω_c is defined according to the following equation:

$$\Omega_c = \sqrt{\frac{K_c}{\gamma_T}} \quad (21)$$

Substitution of the definitions 20 and 21 in Eq.s 14 –17, yields the non-dimensional equations of motion:

$$\varepsilon^2 \frac{\partial^4 \bar{w}_T}{\partial \xi_T^4} + \bar{\kappa}(\xi_T) \bar{w}_T + 2\zeta \frac{\partial \bar{w}_T}{\partial \tau} + \frac{\partial^2 \bar{w}_T}{\partial \tau^2} = \bar{\varrho} \frac{\partial \bar{u}_v}{\partial \tau} + \bar{c}_d \bar{u}_v \quad (22)$$

where $\bar{w}_T = w_T / L_T$, and the following non-dimensional damping coefficient has been introduced:

$$\zeta = \frac{c_v}{2\sqrt{K_c \gamma_T}} \quad (23)$$

as well as the following non-dimensional inertia and drag coefficients:

$$\bar{\varrho} = C_I \frac{\rho_w}{\rho_T} \quad (24)$$

$$\bar{c}_d = \sqrt{\frac{2}{\pi}} C_D \rho_w D_T \sigma_{u_v} \frac{1}{\sqrt{K_C \gamma_T}} \quad (25)$$

being ρ_T the material density of the tube cross-section. Additionally, the symbol $\bar{\kappa}(\xi_T) = K(x_T(\xi_T))/K_c = \tilde{K}(x(\xi_T))$ denotes the non-dimensional stiffness of the mooring system, and ε is the non-dimensional bending stiffness of the tunnel:

$$\varepsilon = \frac{1}{L_T^2} \sqrt{\frac{EI_T}{K_c}} \quad (26)$$

3.2 Solution strategy

As long as the assumptions at the basis of the continuous linear SFT model described in Section 3 can be considered as acceptable, the modal superposition principle can be employed. This allows expressing the non-dimensional transverse displacement through a series expansion in the modal basis of the structure, i.e.:

$$\bar{w}_T(\xi_T, \tau) = \sum_{n=1}^{N} \phi_n(\xi_T)\, \bar{p}_n(\tau) \quad (27)$$

where ϕ_n and $\bar{p}_n$ are, respectively, the n-th mode shape function and the dimensionless modal (or principal) coordinate of the structure and N is a truncation mode number. Approximate solutions of Eq. 22 can be obtained through an application of the Rayleigh–Ritz discretization method. To this aim, the following series expansion of the tunnel mode shapes is introduced:

$$\phi_n(\xi_T) = \sum_{m=1}^{M} \psi_m(\xi_T)\alpha_{n,m} \tag{28}$$

where M and $\alpha_{n,m}$ respectively denote the truncation number and the combination parameters of the series expansion, and the functions ψ_m (with $m = 1, \ldots, M$) are a basis of sufficiently regular shape functions that should satisfy at least the kinematic boundary conditions of the problem (i.e. $\phi(\xi_T = 0) = 0$ and $\phi(\xi_T = 1) = 0$). The shape functions are herein taken equal to the mode shapes of the tunnel restrained by a mooring system with constant stiffness ($\bar{\kappa} = 1\ \forall \xi_T$):

$$\psi_m(\xi_T) = \sin(m\pi\xi_T) \tag{29}$$

By exploiting the orthogonality properties of the shape functions, substitution of Eq. 27 – 29 in Eq. 22 yields, after some straightforward computations, the following system of decoupled ordinary differential equations of motion:

$$\ddot{\bar{p}}_n + 2\nu_n\bar{\omega}_n\dot{\bar{p}}_n + \bar{\omega}_n^2\bar{p}_n = \bar{J}_n(\bar{\varrho}\dot{\bar{u}} + \bar{c}_d\bar{u}) = \bar{J}_n\bar{F}_M(\tau) \tag{30}$$

having denoted with a dot symbol the derivative with respect to the dimensionless time τ and having introduced the scalar coefficients $\bar{J}_n$ according to the following definition:

$$\bar{J}_n = \frac{\sum_{m=1}^{M}\alpha_{n,m}\int_0^1 \psi_m(\xi_T)d\xi_T}{\frac{1}{2}\sum_{m=1}^{M}\alpha_{n,m}^2} \tag{31}$$

The symbols ν_n and $\bar{\omega}_n$ respectively denote the n-th modal damping ratio and the n-th dimensionless natural circular frequency of the system.

At this stage, it is convenient to fully characterize the SFT response in the frequency domain. To this aim, let us introduce the non-dimensional frequency response function (FRF) of mode n:

$$\bar{H}_n(\bar{\omega}) = \frac{1}{-\bar{\omega}^2 + 2i\bar{\omega}\bar{\omega}_n\nu_n + \bar{\omega}_n^2} \tag{32}$$

where i the imaginary unit. The modal coordinates will be then characterized by a non-dimensional covariance matrix with entries:

$$\bar{\sigma}_{p_r p_s} = \bar{J}_r\bar{J}_s\int_{-\infty}^{+\infty}\bar{H}_r(\bar{\omega})\bar{S}_{\bar{F}_M}(\bar{\omega})\bar{H}_s^*(\bar{\omega})d\bar{\omega}, \quad r \neq s \tag{33}$$

where the symbol * has been used to indicate the complex conjugate operator. The n-th non-dimensional variance, instead, reads:

$$\bar{\sigma}_{p_n}^2 = \bar{J}_n^2\int_{-\infty}^{+\infty}|\bar{H}_n(\bar{\omega})|^2\bar{S}_{\bar{F}_M}(\bar{\omega})d\bar{\omega} \tag{34}$$

with the definition:

$$\bar{S}_{\bar{F}_M}(\bar{\omega}) = \bar{\varrho}^2\,\bar{S}_{\dot{\bar{u}}_v}(\bar{\omega}) + \bar{c}_d^2\,\bar{S}_{\bar{u}_v}(\bar{\omega}) \tag{35}$$

being $\bar{S}_{\bar{u}_v}(\bar{\omega})$ and $\bar{S}_{\dot{\bar{u}}_v}(\bar{\omega})$ the dimensionless counterpart of Eq. 10 and 12, respectively. The covariance matrix of the physical displacement is then readily obtained through a linear transformation involving the shape functions matrix of the system. The diagonal terms of the so-obtained matrix are the variances of the physical dimensionless displacement $\sigma_{\bar{w}_T}^2$.

4. LOCAL DYNAMICS

Let us now make reference to Fig. 2 and consider a tether inclined of an angle θ with respect to the horizontal line, having initial chord length L_0, external diameter D_o, mass per unit of length γ_s, axial stiffness EA_0 and subject to a static pretension $T_0 > 0$. Following the same reasoning done in Sec. 3, the "virtual" mass per unit of length of the tether can be expressed as:

$$\gamma_v = \gamma_s + C_A\,\gamma_w \tag{36}$$

where $\gamma_w = \rho_w\pi D_o^2/4$, and $C_A = 1$ in the case of a circular cross-section. The self-weight per unit of length of the tether is denoted by w_s (i.e. $w_s = \gamma_s g$, being g the gravity acceleration), while the symbol br indicates its buoyancy ratio, namely the ratio of the hydrostatic forces per unit of length and the self-weight per unit of length. Furthermore, in the context of small-sag cable

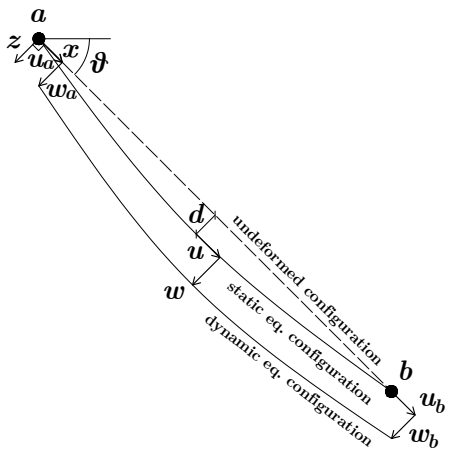

FIGURE 2: Schematic representation of an inclined submerged tether with a general form of supports motion.

theory, let us denote by λ^2 Irvine's well-known elasto-geometric parameter, defined according to the following equation (see [16]):

$$\lambda^2 = \Gamma^2\cos^2(\theta)\,\frac{1}{\varepsilon_0} \tag{37}$$

In the previous expression $\Gamma = w_s(1 - br)L_0/T_0$ has been introduced in compact form, while ε_0 is the initial static axial strain of the tether. The latter quantity can be also expressed as a function of the non-dimensional pretension $\eta_0 = T_0/T_y$:

$$\varepsilon_0 = \frac{T_0}{EA_0} = \frac{\eta_0 T_y}{EA_0} = \frac{\eta_0 f_y}{E} \tag{38}$$

where $T_y = f_y A_0$ is the yielding tensile force and f_y is the yielding stress of the material. The non-dimensional load parameter is directly proportional to the BWR of the SFT (i.e., $\eta_0 \propto$ BWR). The static stress which acts on the tether can be then conveniently expressed as a fraction of the yielding stress, i.e.: $\sigma_s = T_0/A_0 = \eta_0 f_y$. Additionally, the midspan sag d of the inclined anchor can be computed, according to the classic parabolic approximation as:

$$d = \frac{w\, L_0^2}{8\, T_0} \cos\theta = \frac{w_s(1-br)\, L_0^2}{8\, T_0} \cos\theta \tag{39}$$

The main hypothesis of the model is that the total time-dependent displacements of the element can be decomposed into the sum of two parts: the quasi-static component (denoted by the superscript q) and modal component (denoted by superscript m). The former are the displacements of the anchor which moves as an elastic tendon, while the latter are expressed as a combination of the linear undamped modes of a cable with fixed ends. Hence, longitudinal and transverse displacements of the tether respectively read (see [17]):

$$u(x,t) = u^q(x,t) + u^m(x,t) \tag{40a}$$

$$w(x,t) = w^q(x,t) + w^m(x,t) \tag{40b}$$

being x the local abscissa of the tether (see Fig. 2) and t the dimensional time variable. However, as already anticipated in Sec. 1 of the present work, (1) global and local vibrations modes of the SFT are associated to well separated natural frequencies and (2) coupling between the mooring system and the SFT's bare tube is one-way only (i.e. the tube transmits vibrations to the anchors, but not viceversa). For these reasons, the response of the tether subject to hydrodynamic loads can be tackled by considering the case of fixed-supports, which amounts to set $u(x=0,t) = u_a = 0$, $u(x=L_0,t) = u_b = 0$, $w(x=0,t) = w_a = 0$ and $w(x=L_0,t) = w_b = 0$ (see Fig. 2). Within this context, the quasi-static part of the displacements is identically equal to zero, i.e. $u^q(x,t) = w^q(x,t) = 0$. For what concerns the modal motions, the separation of variable is employed for the transverse displacement, whereas the axial modal motion is assumed to be negligible compared to the first one, since it involves frequencies much higher than those associated with the in-plane transverse vibrations:

$$u^m(x,t) \ll |w^m(x,t)| \tag{41a}$$

$$w^m(x,t) = \psi(x) z(t) \tag{41b}$$

The temporal coefficient $z(t)$ can be interpreted as the generalized modal coordinate of the in-plane motion (i.e. the single degree of freedom of the model), whereas $\psi(x)$ is the shape function, which is selected as the first eigenfunction of the taut-string with fixed ends:

$$\psi(x) = \sin(\pi x/L_0) \tag{42}$$

This can be viewed as a special case of a Rayleigh-Ritz discretization procedure, in which only one shape function is retrained.
By applying a standard energetic approach, i.e., writing potential and kinetic energies, it is possible to derive the equation of motion of the fixed-supports tether, which reads:

$$\ddot{z} + 2\xi^s \omega\, \dot{z} + \omega^2\, z + \beta z^2 + \nu z^3 = \frac{2}{\gamma_v L_0} \int_0^{L_0} f_m(x,t)\, \psi(x) dx \tag{43}$$

where the expressions of the coefficients β and ν are reported in App. A. Moreover, in Eq. 43, ξ^s denotes the structural viscous modal damping coefficient, ω is the natural circular frequency (see again App. A), $m = \gamma_v\, L_0/2$ is the modal mass of the tether, while $f_m(x,t)$ is the space and time dependent Morison force per unit of length acting on the anchor, and reads:

$$f_m(x,t) = f_i(x,t) + f_d(x,t) \tag{44}$$

being $f_i(x,t)$ the inertia force per unit of length:

$$f_i(x,t) = C_I \rho_w \pi \frac{D_o^2}{4} \dot{u}_\perp(x,t) = k_i\, \dot{u}_\perp(x,t) \tag{45}$$

and $f_d(x,t)$ the drag force per unit of length:

$$f_d(x,t) = k_d |U_\perp(x) + v_\perp(x,t)| \Big(U_\perp(x) + v_\perp(x,t) \Big) \tag{46}$$

In the previous equations $k_d = C_D\, \rho_w D_o/2$, while C_D and C_I denote, respectively, the drag and inertia coefficient of the cross-section. Moreover, $v_\perp(x,t) = u_\perp(x,t) - \psi(x)\dot{z}(t)$, $\dot{u}_\perp(x,t)$ and $U_\perp(x)$ denote, respectively, the relative fluid-structure velocity, the wave particle acceleration and the current velocity normal to the chord of the tether. In this work, the current velocity profile is modeled as the superposition of a one-seventh power law which represent the tidal current profile, and a linear wind-stress induced profile, namely:

$$U(z) = U_t \left(\frac{z}{d}\right)^{\frac{1}{7}} + U_w \left(\frac{z}{d}\right) \tag{47}$$

being z the same vertical coordinate introduced in Sec. 2 and d the water depth. The symbols U_t and U_w indicate, respectively, the reference velocity of the tidal and wind-induced profile at the water surface. The normal component of the current velocity to the tether's axis is found after simple projection, i.e. $U_\perp(z) = U(z)\sin\theta$. The change of coordinate $z = (L_0 - x)\sin\theta$ leads to wave kinematic quantities and current velocity which are functions of the local tether's abscissa x only. This choice will be hereafter conveniently adopted to deal with the spatial variability of the hydrodynamic load.

4.1 Statistical Cubicization

Being the current profile in general not null, the mean of the response is in general different from zero. The system response can be decomposed as:

$$z(t) = \mu_z + \tilde{z}(t) \tag{48}$$

where μ_z is the mean of the modal coordinate and $\tilde{z}(t)$ is a zero-mean process. Substitution of Eq. 48 into Eq. 43 with subsequent ensemble averaging yields the following algebraic nonlinear equation in the mean of the response:

$$\nu\mu_z^3 + \beta\mu_z^2 + \omega^2\mu_z = < F_D(\dot{z},t) > \tag{49}$$

being:

$$F_D(\dot{z},t) = \frac{2}{\gamma_v L_0} \int_0^{L_0} f_d(x,t)\, \psi(x) dx \tag{50}$$

The nonlinear system can be then approximated by the following equation of motion in the zero-mean modal coordinate $\tilde{z}$:

$$\ddot{\tilde{z}} + 2\xi^s \omega \dot{\tilde{z}} + \omega^2 \tilde{z} + \beta \tilde{z}^2 + \nu \tilde{z}^3 = \tilde{F}_I(t) + \tilde{F}_D(\dot{\tilde{z}}, t) \tag{51}$$

where:

$$\tilde{F}_I(t) = \frac{2}{\gamma_v L_0} \int_0^{L_0} f_i(x,t)\, \psi(x) dx \tag{52}$$

is the linear generalized inertia force (treated in exact form), while the zero-mean generalized modal drag force is given by:

$$\tilde{F}_D(\dot{\tilde{z}}, t) = \frac{2k_d}{\gamma_v L_0} \int_0^{L_0} \psi(x) f_{d,eq}(x,t) dx \tag{53}$$

being $f_{d,eq}(x,t)$ and equivalent zero-mean drag force per unit of length expressed as a cubic polynomial in $\tilde{v}_\perp(x,t) = u_\perp(x,t) - \psi(x)\dot{\tilde{z}}(t)$, which is found after minimizing the error between the original nonlinear system and the current one. The equivalent cubic drag force reads:

$$f_{d,eq}(x,t) = \alpha_1(x)\tilde{v}_\perp(x,t) + \alpha_2(x)\left[\tilde{v}_\perp^2(x,t) - < \tilde{v}_\perp^2(x,t) >\right] + \alpha_3(x)\tilde{v}_\perp^3(x,t) \tag{54}$$

where:

$$\alpha_1(x) = 2U_\perp(x)\, q_1(x) + 2\sqrt{\sigma_{\tilde{v}_\perp}^2}\, q_2(x) \quad \alpha_2(x) = q_1(x) \quad \alpha_3(x) = \frac{2}{3}\frac{q_2(x)}{\sqrt{\sigma_{\tilde{v}_\perp}^2}} \tag{55}$$

being

$$q_1(x) = \mathrm{erf}\left(\frac{U_\perp(x)}{\sqrt{2\sigma_{\tilde{v}_\perp}^2}}\right) \tag{56}$$

and

$$q_2(x) = \frac{1}{\sqrt{2\pi}} \exp\left(-\frac{U_\perp^2(x)}{2\sigma_{\tilde{v}_\perp}^2}\right) \tag{57}$$

where the symbol $< \cdot >$ denotes the mathematical expectation operator. In the previous expressions, $\sigma_{\tilde{v}_\perp}^2$ indicates the variance of the relative zero-mean fluid-structure velocity. Since this quantity is unknown apriori, an iterative solution procedure is required. Further details on the stochastic cubicization procedure can be found, e.g., in [18, 19].

4.2 Non-dimensional formulation

By introducing a set of suitable characteristic quantities, it is possible to write the dimensionless version of the equation of motion by properly scaling space and time variables. Let us denote with L_c a characteristic length of the system and with ω_c a characteristic circular frequency, which are respectively selected as the maximum value of the midspan sag achieved for an equivalent horizontal anchor (i.e., having the two supports at the same level) and as the first in-plane natural circular frequency of the taut-string model:

$$L_c = \frac{w_s(1-br)\, L_0^2}{8\, T_0} = \frac{\Gamma\, L_0}{8} \tag{58}$$

$$\omega_c = \frac{\pi}{L_0}\sqrt{\frac{T_0}{\gamma_v}} \tag{59}$$

Substitution of Eq.s 58 and 59 into Eq. 51 yields the following non-dimensional equation of motion in the zero-mean dimensionless modal coordinate $\tilde{\bar{z}}$:

$$\ddot{\tilde{\bar{z}}} + 2\xi^s \bar{\omega}\, \dot{\tilde{\bar{z}}} + \bar{\omega}^2\, \tilde{\bar{z}} + \bar{\beta}\tilde{\bar{z}}^2 + \bar{\nu}\tilde{\bar{z}}^3 = \tilde{\bar{F}}_I(\tau) + \tilde{\bar{F}}_D(\dot{\tilde{\bar{z}}}, \tau) \tag{60}$$

where the expressions of the non-dimensional coefficients are reported in App. A. Additionally:

$$\tilde{\bar{F}}_I(\tau) = \frac{2L_0}{\pi^2 T_0 L_c} \int_0^{L_0} f_i(x,t)\, \psi(x) dx \tag{61}$$

and:

$$\tilde{\bar{F}}_D(\dot{\tilde{\bar{z}}}, \tau) = \frac{2L_0}{\pi^2 T_0 L_c} \int_0^{L_0} f_{d,eq}(x,t)\, \psi(x) dx \tag{62}$$

are the non-dimensional modal generalized load associated to the zero-mean inertia and drag force, respectively.

4.3 Third-order Volterra Model

To conveniently address both geometrical and load-induced nonlinearities, a third-order Volterra Model of the sdof system is developed. The Associated Linear Equations (ALEs, see e.g. [20]) are easily determined by expressing the system response as a series expansions whose coefficients can be viewed as the integer powers of a book-keeping parameter Λ:

$$\tilde{\bar{z}}(\tau) = \sum_{j=1}^{3} \Lambda^j \tilde{\bar{z}}^{(j)}(\tau) \tag{63}$$

Let us replace $\dot{u}_\perp(x,t)$ by $\Lambda\dot{u}_\perp(x,t)$ and $u_\perp(x,t)$ by $\Lambda u_\perp(x,t)$ into Eq.s 60–62. Equating like powers of Λ, the ALEs read:

$$\ddot{\tilde{\bar{z}}}_1 + 2\bar{\omega}(\xi^s + \xi^{eq})\dot{\tilde{\bar{z}}}_1 + \bar{\omega}^2\tilde{\bar{z}}_1 = \tilde{\bar{F}}_I(\tau) + \tilde{\bar{F}}_D^{(1)}(\tau) \tag{64a}$$

$$\ddot{\tilde{\bar{z}}}_2 + 2\bar{\omega}(\xi^s + \xi^{eq})\dot{\tilde{\bar{z}}}_2 + \bar{\omega}^2\tilde{\bar{z}}_2 = -\bar{\beta}\tilde{\bar{z}}_1^2 + \tilde{\bar{F}}_{D*}^{(2)}(\dot{\tilde{\bar{z}}}_1, \tau) \tag{64b}$$

$$\ddot{\tilde{\bar{z}}}_3 + 2\bar{\omega}(\xi^s + \xi^{eq})\dot{\tilde{\bar{z}}}_3 + \bar{\omega}^2\tilde{\bar{z}}_3 = -2\bar{\beta}\tilde{\bar{z}}_1\tilde{\bar{z}}_2 - \bar{\nu}\tilde{\bar{z}}_1^3 + \tilde{\bar{F}}_D^{(3)}(\dot{\tilde{\bar{z}}}_1, \tau) \tag{64c}$$

The following definition has been introduced:

$$\tilde{\bar{F}}_{D*}^{(2)}(\tau, \dot{\tilde{\bar{z}}}_1) = \tilde{\bar{F}}_D^{(2)}(\tau, \dot{\tilde{\bar{z}}}_1) - < \tilde{\bar{F}}_D^{(2)}(\tau, \dot{\tilde{\bar{z}}}_1) > \tag{65}$$

The equivalent viscous modal damping coefficient ξ^{eq} has been defined as:

$$\xi^{eq} = \frac{K_D}{2\bar{\omega}} \int_0^{L_0} \psi^2(x)\alpha_1(x)dx \tag{66}$$

and physically stems from the dissipative nature of the linear term in the structural velocity, being:

$$K_D = \frac{2L_0 k_d}{\pi^2 T_0 L_c} = \frac{8}{\pi^2} \frac{C_D D_o \rho_w}{T_0 \Gamma} \tag{67}$$

Additionally, rearranging Eq. 61 one simply has:

$$\tilde{\bar{F}}_I(\tau) = K_I \int_0^{L_0} \psi(x)\dot{u}_\perp(x,t)dx \tag{68}$$

being:

$$K_I = \frac{2L_0 k_i}{\pi^2 T_0 L_c} = \frac{4}{\pi} \frac{C_I D_o^2 \rho_w}{T_0 \Gamma} \tag{69}$$

Moreover, the following definitions have been also introduced:

$$\tilde{\bar{F}}_D^{(1)}(\tau) = K_D \int_0^{L_0} \psi(x)\alpha_1(x)u_\perp(x,t)dx \tag{70}$$

$$\tilde{\bar{F}}_D^{(2)}(\dot{\tilde{z}}_1,\tau) = K_D \int_0^{L_0} \psi(x)\alpha_2(x)\left[u_\perp(x,t) - \psi(x)\dot{\tilde{z}}_1\right]^2 dx \tag{71}$$

$$\tilde{\bar{F}}_D^{(3)}(\dot{\tilde{z}}_1,\tau) = K_D \int_0^{L_0} \psi(x)\alpha_3(x)\left[u_\perp(x,t) - \psi(x)\dot{\tilde{z}}_1\right]^3 dx \tag{72}$$

where $\dot{\tilde{z}}_1(t) = L_c\omega_c\,\tilde{\dot{z}}_1(\tau)$. The approximated solution of Eq. 60 can be then computed, according to its Volterra series expansion, as:

$$\tilde{\bar{z}}(\tau) \cong \tilde{\bar{z}}_1(\tau) + \tilde{\bar{z}}_2(\tau) + \tilde{\bar{z}}_3(\tau) \tag{73}$$

4.4 Solution Strategy

The associated linear equations (Eq.s 64) can be attacked in several ways. In this preliminary work, the ALEs are integrated in the time domain by means of the implicit Runge-Kutta scheme (*ode45* in Matlab), within a Monte-Carlo simulations framework. Even though this is not the most convenient methodology solution, it is still more advantageous compared to the solution of the coupled equation of motion (Eq. 43), since the ALEs can be solved in a cascade manner. Moreover, it allows to have a reference solution which serves as a validation of the results obtained adopting different techniques, such as frequency domain methods involving either the numerical solution of multi-fold integrals (see, e.g. [18]) or their closed-form approximation thanks to the application of the Multiple Timescales Spectral Analysis (MTSA) proposed in [21] and adopted, e.g., in [22].

5. APPLICATION EXAMPLE

The present section considers an application example regarding the SFT which was proposed for the crossing of the Messina's strait, in Italy (see e.g. [1, 23]). The considered SFT is designed to connect Sicily to the mainland, crossing a strait characterized by a maximum seabed depth of 325 m (see Fig. 3). The total length of the SFT is $L_T = 4680$ m and the tunnel axis is placed 40 m below the water table. The cross section of the tunnel is defined by the following parameters: $D_T = 15.95$ m, $EI_T = 4.383 \cdot 10^{10}$ kNm^2 and $\gamma_T = 368.41$ ton/m. The drag and inertia coefficient of the tube cross-section are respectively set equal to $C_D = 1.2$ and $C_I = 2$. The mooring system is made of inclined hollow core circular cross-section tethers, located along 65 mooring stations, with uniform spacing $\Delta = 72$ m. For the sake of simplicity, in the present work, the mooring system is considered composed of one hollow circular cross-section only (Type B, see Fig. 3), leading to a mooring stiffness variability which is only induced by the variation of the seabed depth along the tunnel's abscissa (see Fig. 4). The cross-section type B is defined by the following parameters: $D_o = 1.950$ m, $A_0 = 0.3849$ m^2, $\gamma_v = 6005$ kg/m and $br = 0.98$. The angle of inclination and the non-dimensional pretension of the anchoring elements are set respectively to $\theta = 135°$ and $\eta_0 = 10\%$.

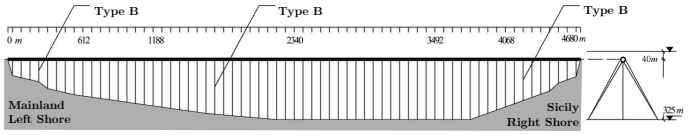

FIGURE 3: Schematic representation of the proposal for the Messina's strait SFT (side view and cross-section).

5.1 Global Response of the SFT

The global response of the SFT is first tackled by means of the model presented in Sec. 3, adopting the spectral solution strategy. For the sake of simplicity, the spatial correlation of the water particle velocities along the tunnel's abscissa ξ_T is neglected, as a conservative choice, consistently with the formulation presented in Sec. 3. Figure 5 and 6 depict the standard deviation of the tunnel's transverse displacement obtained by considering a PSD of the wave elevation computed for a significant wave height $H_s = 16$ m. Figure 5 shows the standard deviation of the tunnel displacement for two different profiles of the mooring stiffness (see also Fig. 4). It is highlighted that, for the case of real stiffness profile, maximum values of σ_{w_T} are reached in the "plateau" zone,

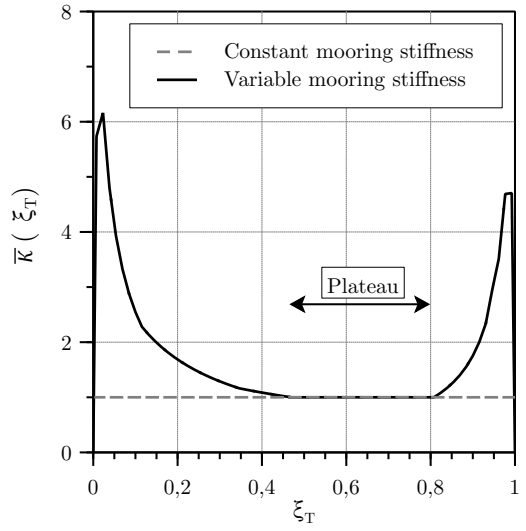

FIGURE 4: Non-dimensional mooring stiffness ($\bar{\kappa}(\xi_T)$) profiles for the Messina's strait SFT proposal.

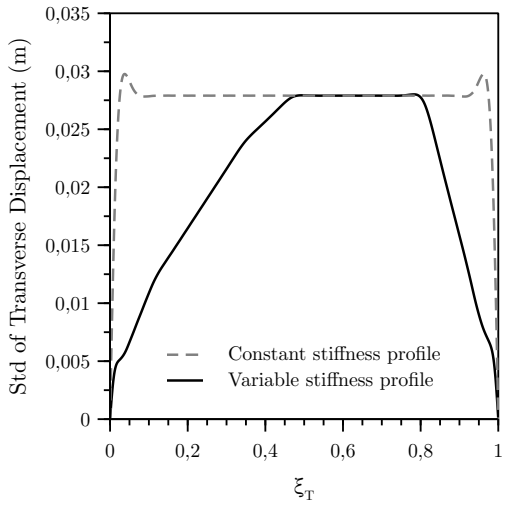

FIGURE 5: Standard deviation of the transverse displacement of the tube obtained considering the complete Morison force. Comparison with two different stiffness profiles.

i.e. in the region where the mooring stiffness is minimum, i.e. for $\xi_T \in [0.45, 0.8]$ (compare with Fig. 4). Moreover, Fig. 6 shows the values of σ_{w_T} obtained by considering the inertia force and the drag force separately, as a comparison with the results obtained considering the total Morison force (i.e. both drag and inertia, see Eq. 15). As it can be clearly appreciated, the motion regime is inertia-dominated. The drag force contribution on the physical response is totally negligible compared to the one stemming from the inertia force.

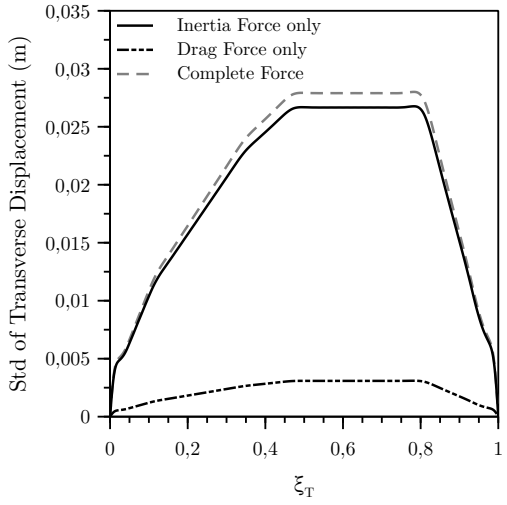

FIGURE 6: Standard deviation of the transverse displacement of the main tube obtained considering the Inertia force (see Eq.s 15 and 16) and the Drag force (see Eq.s 15 and 17) separately.

5.2 Local Response of the Tether

In this subsection, the Type B inclined tether designed for the Messina's strait SFT proposal is considered. The drag and inertia coefficient are respectively set equal to $C_D = 1$ and $C_I = 2$, while the nondimensional pretension is set to $\eta_0 = 10\%$, leading to $\lambda^2 = 0.178$. The structural viscous damping coefficient is assumed equal to $\xi^s = 0.1\%$. Time histories of water particle velocities and accelerations are generated starting from the PSD of the wave elevation, considering a significant wave height $H_s = 16$ m, which is tentatively assumed to represent an extreme hydrodynamic event for the specific site. Moreover, a reference current velocity $U_t = 0.49$ m/s and $U_w = 0.21$ m/s at the water surface are respectively selected for the tidal and wind-stress induced currents. A total of 40 generation stations are considered along the element's length. Preliminary analyses carried out by the authors suggest that for the considered example, this number of stations is sufficient to capture with good accuracy the spatial variation of the load along the developed length of the tether. Time histories of 4000 s duration (which are sufficient to reach a steady-state response) are considered, and iterations are carried out up to convergence of the variance of the relative fluid-structural velocity (i.e. $\sigma^2_{\tilde{v}}$). Within the spirit of Monte Carlo methods, 80 simulations are performed, in order to take statistics of the response.

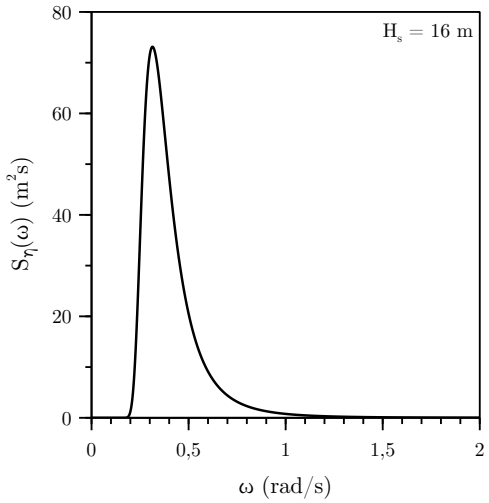

FIGURE 7: Power Spectral Density of the wave elevation, for $H_s = 16$ m.

Figure 7 and 8 depicts, respectively, the PSD of the input wave elevation $S_\eta(\omega)$ and the PSD of the dimensional (zero-mean) modal coordinate $S_{\tilde{z}}(\omega)$ reconstructed from the time histories of the Monte Carlo simulation of the third-order Volterra Model. Moreover, Tab. 1 collects the mean values of the statistics computed for each Monte Carlo simulation, namely the standard deviation of the dimensionless modal coordinate $\sigma_{\tilde{z}}$, the skewness coefficient γ_3 and the excess of kurtosis (i.e. the coefficient of excess) γ_4. It can be clearly appreciated that, for the selected level of the load input, the response is skewed but the coefficient of excess is very close to zero. Moreover, the response of the tether turns out to be mostly resonant, being its natural circular frequency very close to the frequency content of the peak spectral ordinates of PSD of the water kinematic quantities.

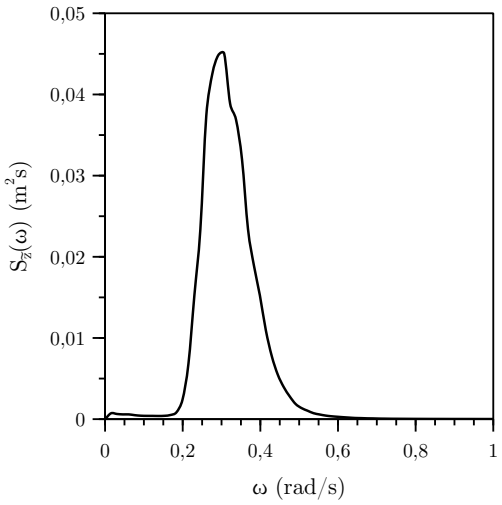

FIGURE 8: Power Spectral Density of the dimensional zero-mean modal coordinate, reconstructed from the Monte Carlo simulation of the associated linear equations (see Eq.s 64 and 73).

TABLE 1: Statistics of the non-dimensional zero-mean modal coordinate $\tilde{\tilde{z}}$ obtained for the Monte Carlo simulation (see Eq.s 64 and 73).

Quantity	Mean Value
Standard Deviation $\sigma_{\tilde{z}}$	0.26
Skewness Coefficient γ_3	0.038
Coefficient of Excess γ_4	0.003

Even though further parametric analyses by varying intensity of the load should be carried out, the application example allows to appreciate the non-gaussianity of the response due to both load-induced and structural (geometrical) nonlinearities. Both sources of nonlinearities are fully accounted for by the third-order Volterra Model presented in this work.

6. CONCLUSIONS

In this work both the global and the local dynamic response of Submerged Floating Tunnels subject to hydrodynamic loads have been investigated. The in-plane global response of the system has been conveniently addressed by modeling the tube as an Euler-Bernoulli beam resting on a non-homogeneous Winkler's bed, representing the variable stiffness provided by the mooring system along the tunnel's abscissa. The local response of the anchoring elements has been tackled by considering a third-order Volterra representation of the single degree of freedom model of a submerged taut inclined tether, accounting for geometrical nonlinearities. The associated linear equations have been analytically derived and numerically solved within a classical Monte Carlo simulation approach, paving the way for the adoption of further advanced solution techniques in the frequency domain.

APPENDIX A. COEFFICIENTS OF THE ANCHOR EQUATION OF MOTION

Dimensional coefficients of Eq. 43 read:

$$\omega = \frac{\pi}{L_0}\sqrt{\frac{T_0}{\gamma_v} + \frac{8T_0\,\lambda^2}{\pi^4\,\gamma_v}} \tag{74}$$

$$\beta = \frac{6\,\pi w_s(1-br)\cos\theta}{4L_0\varepsilon_0} \tag{75}$$

$$\nu = \frac{EA_0\pi^4}{8L_0^3} \tag{76}$$

Their dimensionless counterparties of Eq. 60 instead read:

$$\bar{\omega} = \frac{\omega}{\omega_c} = \sqrt{1 + \frac{8\lambda^2}{\pi^4}} \tag{77}$$

$$\bar{\nu} = \frac{\nu\,L_c^2}{\omega_c^2\,m} = \frac{\pi^2}{256\cos^2\theta}\,\lambda^2 \tag{78}$$

$$\bar{\beta} = \frac{\beta L_c}{\omega_c^2\,m} = \frac{3}{8\pi\cos\theta}\,\lambda^2 \tag{79}$$

REFERENCES

[1] Bruschi, R., Giardinieri, V., Marazza, R. and Merletti, T. "Submerged buoyant anchored tunnels: Technical solutions for the fixed link across the Strait of Messina, Italy." Krokeborg, J. (ed.). *Strait Crossings*: pp. 605–612. 1990. Balkema, Rotterdam.

[2] Fogazzi, P. and Perotti, F. "The dynamic response of seabed anchored floating tunnels under seismic excitation." *Earthquake Engineering and Structural Dynamics* Vol. 29 (2000): pp. 273–295.

[3] Mazzolani, F.M., Landolfo, R., Faggiano, B., Esposto, M., Perotti, F. and Barbella, G. "Structural Analyses of the Submerged Floating Tunnel Prototype in Qiandao Lake (PR of China)." *Advances in Structural Engineering* Vol. 11 (2008): pp. 439–454.

[4] Jakobsen, B. "Design of the Submerged Floating Tunnel operating under various conditions." *Procedia Engineering* Vol. 4 (2010): pp. 71–79.

[5] Mirzapour, J., Shahmardani, M. and Tariverdilo, S. "Seismic response of submerged floating tunnel under support excitation." *Ships and Offshore Structures* Vol. 12 (2017): pp. 404–411.

[6] Foti, F., Martinelli, L. and Perotti, F. "A semi-analytical model for the design and optimization of SFTs under seismic loading." Ramon Casas, J., Frangopol, D.M. and Turmo, J. (eds.). *Bridge Safety, Maintenance, Management, Life-Cycle, Resilience and Sustainability (IABMAS 2022)*: pp. 1117–1121. 2022. CRC Press, London.

[7] Xie, J., Li, J., Chen, J. and Xu, Q. "Seismic response analysis of submerged floating tunnel considering non-uniform excitation and flexible-support boundary effect." *Ocean Engineering* Vol. 286 (2023): p. 115486.

[8] Corazza, S., Geuzaine, M., Foti, F., Denoël, V. and Martinelli, L. "On the Seismic Response of Anchoring Elements for Submerged Floating Tunnels." Gattulli, V., Lepidi, M. and Martinelli, L. (eds.). *Lecture Notes in Civil Engineering*, Vol. 399: pp. 303–313. 2023. Springer Nature.

[9] Torres-Alves, G.A., Hart, C.M.P, Morales-Napoles, O. and Jonkman, S.N. "Structural reliability analysis of a submerged floating tunnel under copula-based traffic load simulations." *Engineering Structures* Vol. 269 (2022): pp. 114752: 1–19.

[10] Yang, Y., Xiang, Y. and Gao, C. "Vehicle-SFT-current coupling vibration of multi-span submerged floating tunnel, part I: mode superposition and Galerkin hybrid method." *Ocean Engineering* Vol. 247 (2022): pp. 110746: 1–18.

[11] Corazza, S., Foti, F. and Martinelli, L. "Dynamic substructuring technique for submerged floating tunnels." Jensen, J.S., Frangopol, D.M. and Schmidt, J.W. (eds.). *Bridge Maintenance, Safety, Management, Digitalization and Sustainability*: pp. 1029–1036. 2024. CRC Press/Balkema.

[12] Wilson, J.F. *Dynamics of offshore structures*. Wiley Inc, Hoboken (1984).

[13] Chakrabarti, S.K. *Hydrodynamics of offshore structures*. Computational Mechanics Publications, Springer, Berlin (1987).

[14] Foti, F., Martinelli, L., Morleo, E. and Perotti, F. "Dynamic response of Submerged Floating Tunnels: An enhanced semi-analytical approach." *Ocean Engineering* Vol. 294 (116648) (2024).

[15] Borgman, L.E. "Random Hydrodynamic Forces on Objects." *The Annals of Mathematical Statistics* Vol. 38 (1967): pp. 37–51.

[16] Irvine, H.M. *Cable Structures*. The MIT Press Cambridge, The MIT Press Series in Structural Mechanics, Massachusetts and London, England (1981).

[17] Warnitchai, P., Fujino, Y. and Susumpow, T. "A non-linear dynamic model for cables and its application to a cable-structure system." *Journal of Sound and Vibration* Vol. 187 No. 4 (1995): pp. 695–712.

[18] Li, X., Quek, S. and Koh, C. "Stochastic Response of Offshore Platforms by Statistical Cubicization." *Journal of Engineering Mechanics* Vol. 121 No. 10 (1995): pp. 1056–1068.

[19] Kareem, A., Zhao, J. and Tognarelli, M.A. "Surge response statistics of tension leg platforms under wind and wave loads: a statistical quadratization approach." *Probabilistic Engineering Mechanics* Vol. 10 (1995): pp. 225–240.

[20] Vazquez Feijoo, J.A., Worden, K. and Stanway, R. "Associated Linear Equations for Volterra operators." *Mechanical Systems and Signal Processing* Vol. 19 (2005): pp. 57–69.

[21] Denoël, V. "Multiple timescales spectral analysis." *Probabilistic Engineering Mechanics* Vol. 39 (2015): pp. 69–86.

[22] Denoël, V. and Carassale, L. "Response of an oscillator to a random quadratic velocity-feedback loading." *Journal of Wind Engineering and Industrial Aerodynamics* Vol. 147 (2015): pp. 330–344.

[23] Perotti, F., Foti, F., Martinelli, L. and Tomasin, M. "SFTs under dynamic loads: new design issues and numerical simulation." *Maintenance, Safety, Risk, Management and Life-Cycle Performance of Bridges (IABMAS 2018)*: pp. 885–892. 2018. Taylor & Francis Group, London, UK.